

B. Denis · R. Laprise · D. Caya

Sensitivity of a regional climate model to the resolution of the lateral boundary conditions

Received: 21 September 2001 / Accepted: 22 April 2002 / Published online: 30 August 2002
© Springer-Verlag 2002

Abstract The sensitivity of a one-way nested regional climate model (RCM) to the spatial and temporal levels of information provided at its lateral boundaries is studied. To unambiguously address these two issues, a perfect-prognosis approach called the Big-Brother Experiment (BBE) is employed. It consists in first establishing a reference climate simulation (called the Big Brother) over a large domain and then using the simulated data for nesting another RCM (called Little Brother) integrated over a smaller domain. The effect of degrading the resolution of lateral boundary conditions (LBC), spatially and temporally, is investigated by comparing the big- and little-brother climate statistics for the total and fine-scale components of the fields, as well as for their stationary and transient components. Within the BBE framework using a 45-km grid-point RCM, it is found that the one-way nesting approach gives satisfactory results for most fields studied when spatial resolutions degraded by up to a factor of 12 are imposed between the nesting data and the Little Brother. For the LBC update interval, 12 h appears to be the upper limit, while little difference is found between update intervals of 3 and 6 h.

1 Introduction

The one-way nesting strategy has been so far the most popular approach employed by dynamical regional

climate models (RCMs) for downscaling large-scale atmospheric information to regional scales. The fine-scale features that develop in RCMs are the results of atmospheric internal dynamical interactions and surface forcings supported by the RCM's high-resolution grid-mesh, while the RCM's large-scale destiny remains controlled by the large-scale atmospheric circulation imposed at its lateral boundaries. The RCM's fine-scale features are the added-values over conventional low-resolution global climate models (GCMs), which are computationally prohibitive to run for long climate simulations with the same high resolution since they have to be integrated with a domain covering the entire Earth.

Even though the one-way nesting technique has become widely used for regional climate modelling and proved to be a workable approach for climate downscaling (Giorgi and Mearns 1999), skepticism has been expressed concerning the ability of such a technique to adequately simulate regional climates (CAS/JSC WGNE 1999, 2000). There are a number of issues that are related to the one-way nesting, which, as the name implies, does not allow feedback between the RCM and its driving data (simulated or objective analyses). Most of these have been reviewed by Denis et al. (2002b) who designed an experimental framework, called the Big-Brother Experiment (BBE), to test the downscaling ability of a one-way nested RCM. From the list of issues raised, the impact of the resolution difference between the driving data and the RCM, and the temporal updating frequency of the lateral boundary conditions (LBC), are two important topics that have not yet been rigorously studied. Here, we propose to use the BBE to shed some light on these two issues.

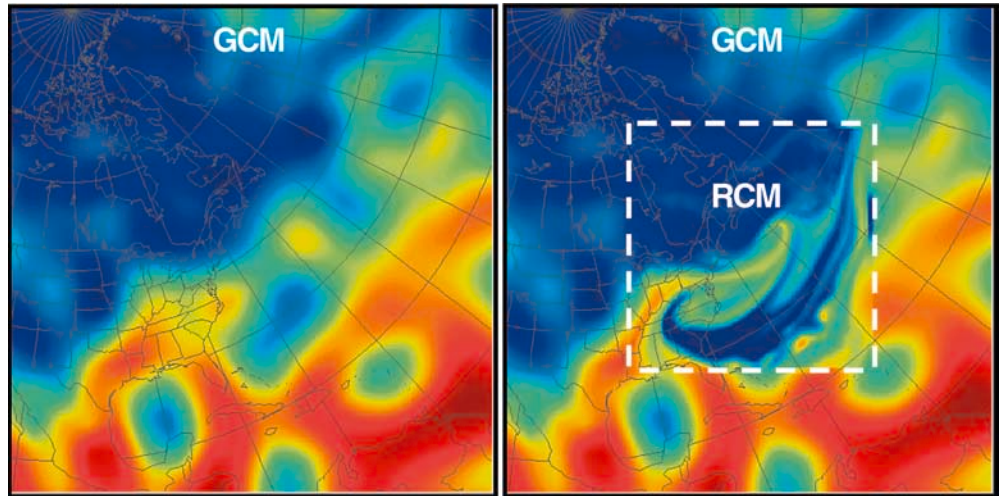
The first objective is to answer the question: what is the maximum difference (or jump) of spatial resolution between the driving data and the driven model that can be used? Figure 1 shows an example of a resolution jump and the implied increased level of details generated by a one-way nested RCM. The case displayed is a

B. Denis (✉) · R. Laprise · D. Caya
Département des sciences de la Terre et de l'Atmosphère,
Université du Québec à Montréal, Montréal, Québec, Canada
E-mail: Bertrand.Denis@ec.gc.ca

B. Denis
Also at: Department of Atmospheric and Oceanic Sciences,
McGill University, Montréal, Québec, Canada

B. Denis
Also at: Meteorological Service of Canada,
Dorval, Québec, Canada, H9P 1J3

Fig. 1 Fine-scale feature generation from a one-way nested RCM. *Left:* GCM at T32 (600 km) resolution. *Right:* a 45 km-resolution RCM nested in the T32 GCM. The field shown is a winter snapshot of low-level specific humidity



winter snapshot of the low-level moisture field produced by the Canadian RCM (CRCM) (Caya and Laprise 1999) nested in the Canadian GCM (McFarlane et al. 1992). In this case, the driving model (GCM) was a spectral T32 (~ 600 km grid spacing) and the nested RCM had a resolution of 45 km. Regional climate simulations using this resolution with the CRCM are reported in Laprise et al. (1998). It can be seen in Fig. 1 that the RCM is able to generate fine-scale features on the large-scale flow imposed at its lateral boundaries. Are these features meaningful and reliable? Or are they just noise and do not make sense from a climate point of view? In other words, are the climate statistics of these features, such as time-averages, transients, extremes and all climate related budgets, realistic? This is the question that Denis et al. (2002b) attempted to answer but with only a single difference of resolution. Here the first objective is to assess the *maximum* difference of resolution that still produces meaningful results. The second objective is to estimate the upper limit of the LBC temporal updating interval that can be employed without deteriorating unacceptably the simulated RCM climate.

2 Experimental design

2.1 The Big-Brother Experiment

Because the validation of RCMs is severely limited by the lack of high-resolution detailed climatologies, a “perfect-prognosis” approach nick-named the Big-Brother Experiment (BBE) is adopted, following the methodology described in detail by Denis et al. (2002b). To summarize, the BBE consists in first establishing a reference climate by performing a large-domain high-resolution RCM simulation (the Big Brother). This reference simulation is then degraded by filtering short scales that are unresolved in today’s global objective analyses (OA) and/or GCMs when integrated for climate projections. This filtered reference is then used to drive the same nested RCM (the Little Brother), integrated at the same high-resolution as the Big Brother, but over a smaller domain that is embedded in the big-brother domain. The climate statistics of the Little Brother are then compared with those of the Big Brother over the little-brother domain. Differences can thus be attributed unambiguously to errors associated with the nesting and

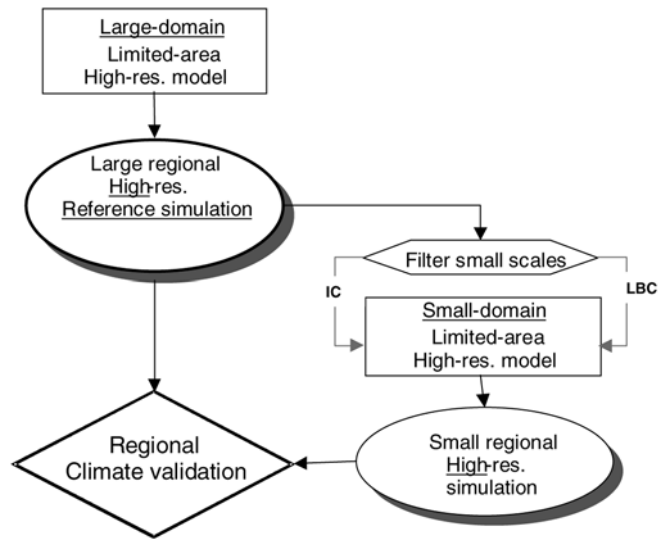


Fig. 2 Simplified flowchart illustrating the BBE framework. Rectangles are the models and ovals are the datasets. The diamond represents validation of the little-brother regional-scale features against those existing in the reference big-brother dataset. The initial conditions (IC) and lateral boundary conditions (LBC) for the small-domain model (right branch) are spatially filtered such that the smallest scales are removed

downscaling technique, and not to model errors nor to observation limitations. The flowchart in Fig. 2 illustrates the essence of the BBE framework. Although not explicitly shown in Fig. 2, the Big Brother has to be supplied with lateral boundary conditions (LBC). This was done with the use of 12-hour archived global analyses. Figure 3 shows the computational domains of the Big and the Little Brother used in this study. The domains are centered on the North-American east coast. The grid-point spacing is 45 km. The big- and little-brother domains include 196 by 196 and 100 by 100 gridpoints, respectively. The little-brother nesting zone is shown as a dashed line along its lateral boundary. The simulations that we shall study are for winter months (four February months).

2.2 Brief description of the CRCM

The RCM employed for the BBE is the Canadian Regional Climate Model (CRCM) (Caya and Laprise 1999). It is a limited-area grid-

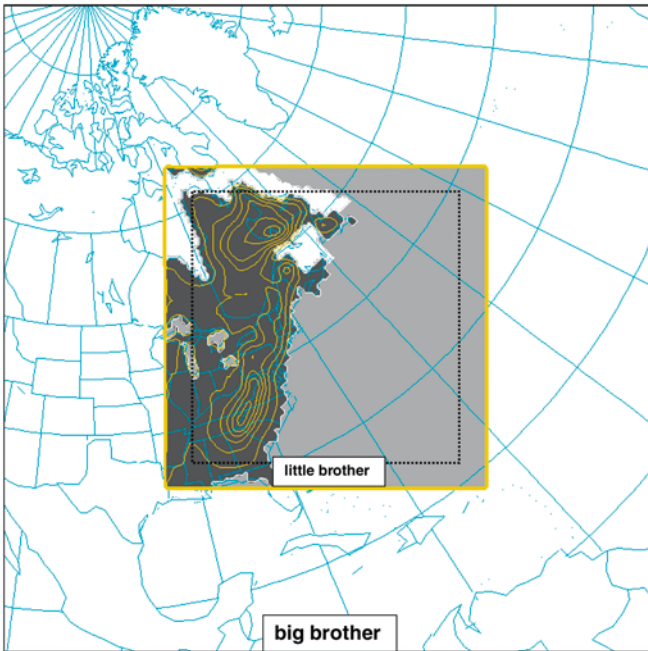


Fig. 3 Large big-brother domain and nested smaller little-brother domain, over north-eastern America. The dashed line around the little-brother domain represents the width of the nesting zone. The topographic field and the land/open-water/sea-ice masks are also shown but only for the Little Brother for clarity. The topography is contoured at every 100 m. Open-water areas are grey and sea-ice areas are white

point non-hydrostatic model that uses a three-time-level semi-Lagrangian semi-implicit numerical scheme. The time step used in our experiments was 15 min and the grid-point spacing 45 km. The one-way nesting technique was developed by Robert and Yakimiw (1986) and Yakimiw and Robert (1990) and is inspired by Davies (1976). A complete description of the dynamical formulation of the CRCM, including the nesting implementation, can be found in Bergeron et al. (1994) and in Laprise et al. (1997). The physical parametrisations are similar to those found in Caya and Laprise (1999) except for the moist convection scheme, which now follows the Kain and Fritsch (1990) formulation (Paquin and Caya 2001). The time evolution of the sea-surface temperature (SST) was imposed by linearly interpolating monthly mean climatological data; because of this, there were no fine-scale structures in the SST field.

2.3 Definition of the spatial resolution jump ratio

In Denis et al. (2002b), the downscaling ability of the one-way nesting was tested for only one resolution jump. The big-brother reference run was degraded such that all disturbances having wavelengths smaller than 500 km were removed while wavelengths greater than 1000 km were left unaffected by the filtering. The grid-point spacing of the RCM being 45 km, the resolution jump defined by the ratio $J = \frac{\text{RCM spatial res.}}{\text{LBC spatial res.}}$ was about 6, i.e., $\sim (\text{wavelength of } 500 \text{ km}) / (\text{wavelength of } 2 \times 45 \text{ km})$. The results for that particular ratio were generally very good.

In the present work, the climate sensitivity to the resolution jump is examined by varying the resolution level of information provided by the LBC. The spatial filtering employed to degrade the resolution has been performed in the spectral space using a 2D discrete cosine transform (DCT) (Denis et al. 2002a). This spectral filtering technique is suitable for non-periodic data and gives full control over the choice of the wavelengths to be removed. Four different resolution jumps have been generated by the filtering of

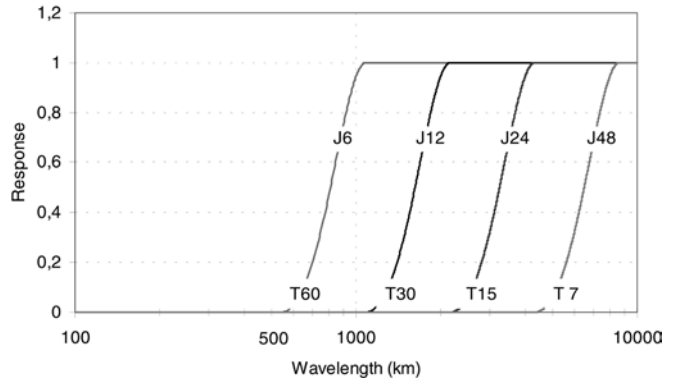


Fig. 4 Response curves of the spectral filter used to degrade the resolution of the driving data. The four resolution jump ratios are labelled J6, J12, J24 and J48 (jump of 6, 12, 24 and 48 times the original 45-km grid resolution). The corresponding spectral triangular spherical truncations T60, T30, T15 and T7, are also given for reference; they have been loosely deduced by dividing the Earth circumference by the truncation number

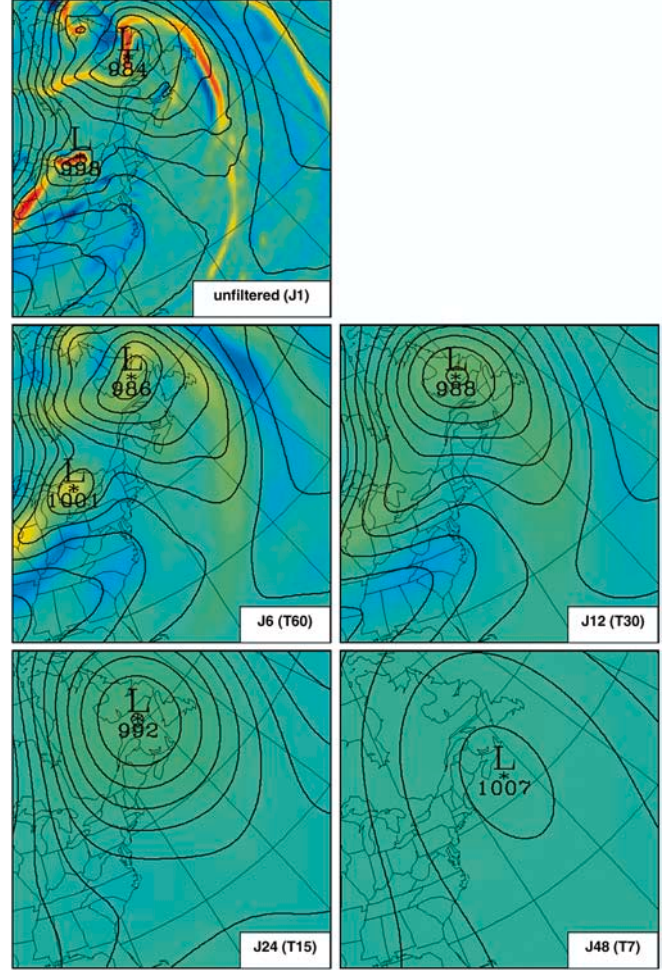


Fig. 5 Examples of filtering corresponding to the response curves of Fig. 4. On each panel the sea-level pressure field is shown with contours and the relative vorticity field is in grey tones. The atmospheric situation is a snapshot of a simulated February 1993. The domain corresponds to the little-brother domain

the big-brother dataset. Figure 4 shows the response curves defining the four resolutions. The corresponding resolution jump ratios (J_6 , J_{12} , J_{24} and J_{48}) for the 45-km RCM and the equivalent spectral triangular spherical harmonic truncations (T_{60} , T_{30} , T_{15} and T_7) are also shown. As an illustration of the filtering effect, Fig. 5 shows the results of the four filtering levels on an instantaneous mean-sea-level pressure field and a relative vorticity field (1000 hPa). The panel labelled J1 displays the unfiltered fields. For all spatial resolution experiments, the temporal updating interval was 3 h. Linear time-interpolation was performed between these times to accommodate the nesting which is applied every time step.

2.4 Definition of the temporal updating frequency

In the second part of this study, four updating frequencies will be compared: U8, U4, U2 and U1, corresponding to 8, 4, 2 and 1

Table 1 List the experiments performed in this work. The first column of Xs shows the simulations performed for studying the impact of the spatial resolution jump ratio between the LBC and the Little Brother; the first row of Xs is for studying the impact of the temporal update frequency of the LBC. The Ys are additional experiments for testing the effect of the temporal update frequency on a 45-km grid-point RCM that would be driven by T30 resolution data

	U8 (3 h)	U4 (6 h)	U2 (12 h)	U1 (24 h)
J1	X	X	X	X
J6 (T60)	X			
J12 (T30)	X	Y	Y	Y
J24 (T15)	X			
J48 (T7)	X			

updates per day, i.e. update intervals of 3, 6, 12 and 24 h, respectively. It is important to stress again that linear interpolation is used to fill in between these update instants. The ensemble of experiments that have been performed by varying either the spatial or temporal LBC resolutions, or both, is shown in Table 1.

3 Results

Before looking at the Little-Brother's ability to reproduce the Big-Brother climate when the resolution jump and updating frequency are varied, we would like first to give an idea of the inter-annual variability of the four simulated months. To this end, and to improve the significance of the climate statistics as well as the robustness of the results obtained by Denis et al. (2002b), simulations were carried out for four different February months: February 1990, 1991, 1993 and 1994. Figures 6 and 7 show the big-brother monthly means of sea-level pressure and precipitation rate, respectively. These fields, as well as all the rest of the displayed fields, are shown on the little-brother domain. It can be seen from Figs. 6 and 7 that the inter-annual variability is fairly high, but some characteristics proper to the North American east coast winter climate are noticeable. For example, the pressure trough offshore accompanied by a more intense precipitation area over the ocean is very visible. This is due to the mean circulation producing dry cold air advection over the Gulf Stream which fuels

Fig. 6 Big-brother monthly-mean sea-level pressure for February of 1990, 1991, 1993 and 1994. Contours are at every 2 hPa. Areas with values lower than 1010 hPa are shaded. The fields are shown on the little-brother domain

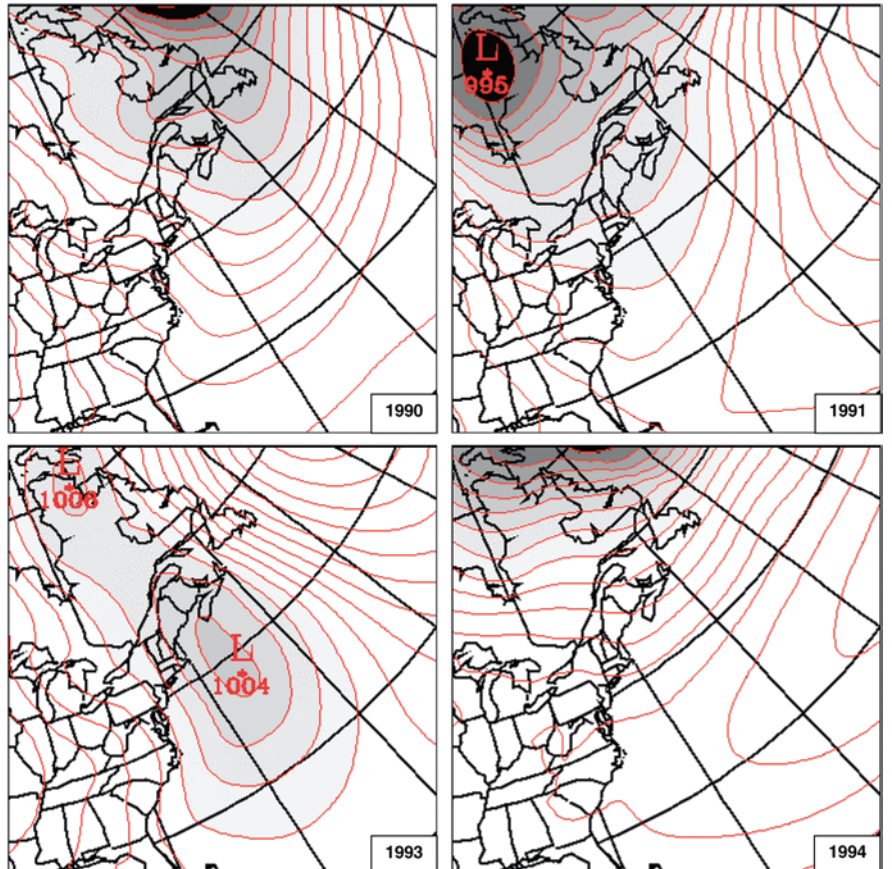
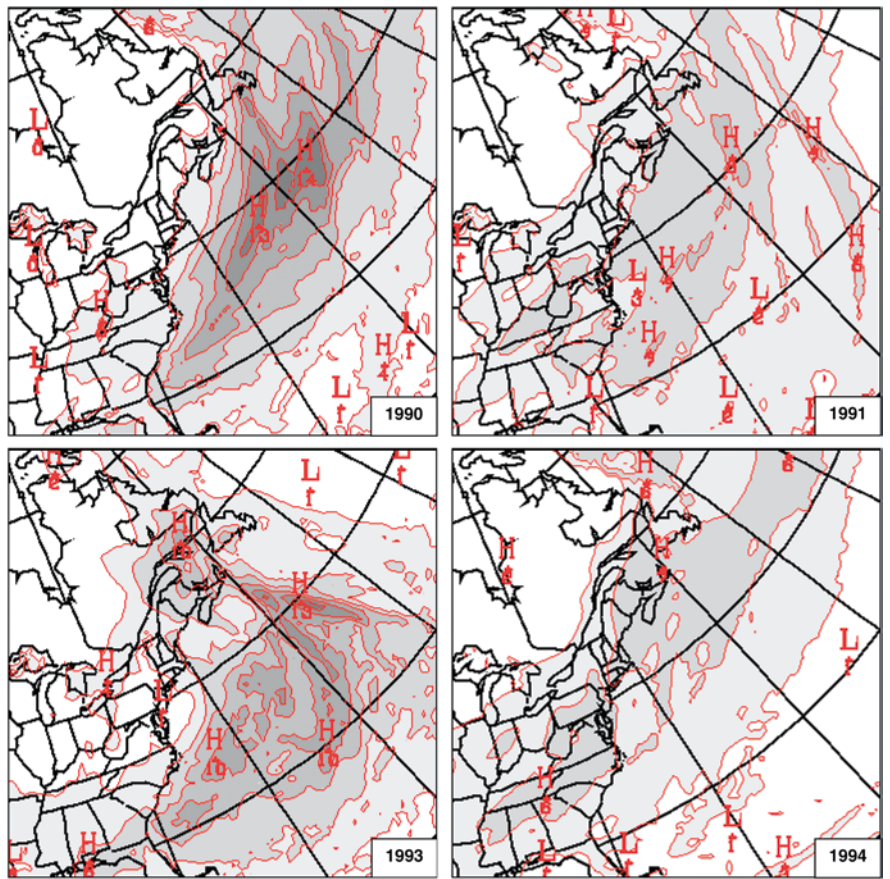


Fig. 7 Big-brother monthly-mean precipitation rates for February of 1990, 1991, 1993 and 1994. Contours are at every 2 mm per day. Areas with values higher than 2 mm per day are shaded



storm developments. Furthermore, the stationary effect of the Great Lakes can be clearly seen by the presence of a trough in the monthly-mean sea-level pressure field of years 1990 and 1993, and also by the increased precipitation over or near them for years 1990, 1991 and 1993.

3.1 Sensitivity to the spatial resolution of the LBC

We now turn our attention to the ability of the Little Brother to reproduce its Big Brother, as a function of the resolution jump ratios as defined in Sect. 2.3. Results are presented first for the time-average (stationary) and time-standard-deviation (transient) parts of sea-level pressure (*slp*) and precipitation rate (*pcp*) fields. The calculations of these time statistics for each experiment were performed after joining up the model output (archived every 3 h) of the February month of the four years; the transient parts include the inter-annual and the intra-monthly variability. In order to facilitate the examination of the little-brother downscaling ability to reproduce the fine-scale features, these features were extracted by the use of a spatial spectral filter (as in Denis et al. 2002b) and examined separately. It must be noted that the fine scales considered here for diagnostic purposes, are those that can survive a J6 filtering. These fine scales had to be regenerated inside the domain by the little-brother simulations (J6, J12, J24, J48); none of

these simulations got information having scales smaller than the J6 level from the lateral boundaries or the initial conditions. For each displayed field, the correlation coefficients (**R**) between each Little Brother and the reference Big Brother are given, as well as the ratios of the spatial variance (Γ). It must be noted that the nesting zone is excluded from all diagnostic calculations or skill scores (such as the correlation coefficients and ratios of variance), but it is part of all field displayed (see Fig. 3 for the nesting zone delimitation). Diagrams summarising the results for the *slp*, *pcp*, and also for 975-hPa temperature and 500-hPa relative vorticity are presented at the end of the section. Finally, because of the small number of realisations (four February per resolution jump), no attempt to test the statistical significance of the results has been made.

3.1.1 Sea level pressure fields

Figures 8 and 9 show the total and the small-scale components of the sea-level-pressure (*slp*) fields averaged over four February months. These fields can be seen as the stationary parts of the mass field even though there exists a non-negligible inter-annual variability for the total components as seen from Fig. 6. The first striking evidence from Fig. 8 is that, as far as the large scale is concerned, the Little Brother is capable of

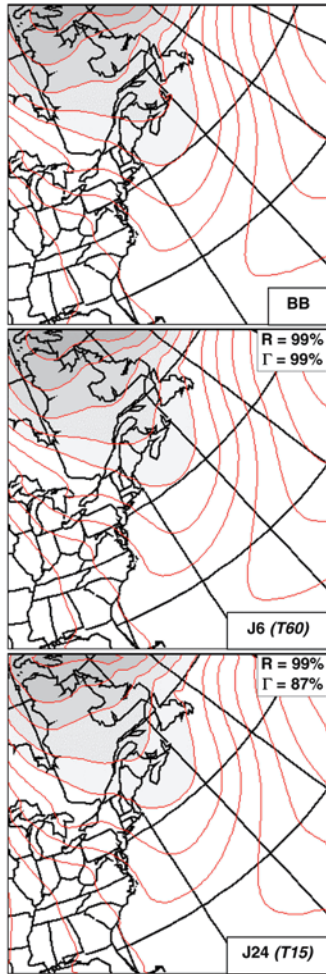


Fig. 8 Sea-level pressure (*slp*) fields averaged over four February months. Contours are at every 2 hPa. Areas with values lower than 1010 hPa are shaded. The resolution jumps (*J*), as well as the corresponding spherical triangular truncations (*T*), are indicated on the *lower-right corners*. Correlation coefficients (*R*) and variance ratios (Γ) between the little-brother and big-brother panels are indicated in the *upper-right corners*

reproducing its Big Brother at least up to a resolution jump ratio of 24 (T15). This may not be surprising since that field is largely dominated by large-scale features which in turn are highly controlled by the large-scale driving LBC provided by the Big Brother. Figure 9 shows that, even though the correlation coefficient for the small-scale components drops faster than for the total component, the fine-scale features, such as those induced by the Great Lakes and the mountains, exhibit a strong robustness up to J24.

The ability to reproduce the transient variability is certainly as important as the ability to reproduce the stationary time-averaged climate. Figure 10 shows the effect of the resolution degradation on the transient-eddy standard deviation of the *slp*. We can see that the Little Brother is capable of maintaining the same level of transient activity as its Big Brother, and that up to J12. After this jump of resolution the activity is significantly

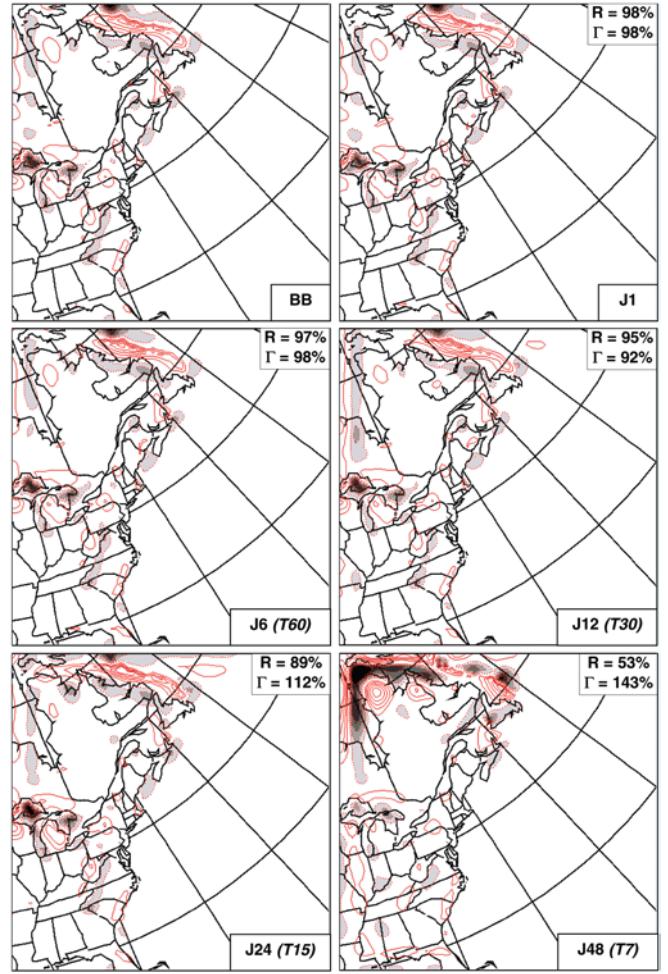


Fig. 9 Stationary small-scale component of *slp* (over four February months). Contour intervals are at every 0.1 hPa. The zero contour is omitted for clarity. Correlation coefficients (*R*) and variance ratios (Γ) between the little-brother and big-brother panels are in the *upper-right corners*

smaller, as shown by a variance ratio Γ of 70% and 12% for J24 and J48, respectively. Interestingly, when only the fine scales are considered in the calculation of the transient activity (Fig. 11), the Little Brother yields reasonable results up to J24.

3.1.2 Precipitation rate fields

Precipitation is probably one of the most important climate quantities. It is also an end-of-the-line product of the climate system since it results from many processes and interactions between the climate components. In an RCM, precipitation is generated by parametrised physical processes as well as numerically resolved atmospheric transports. It is also worth noting that precipitation is not one of the variables that are supplied at the lateral boundaries as are, for example, the pressure, temperature, moisture and wind fields. It is crucial for our study, therefore, that we look at this field.

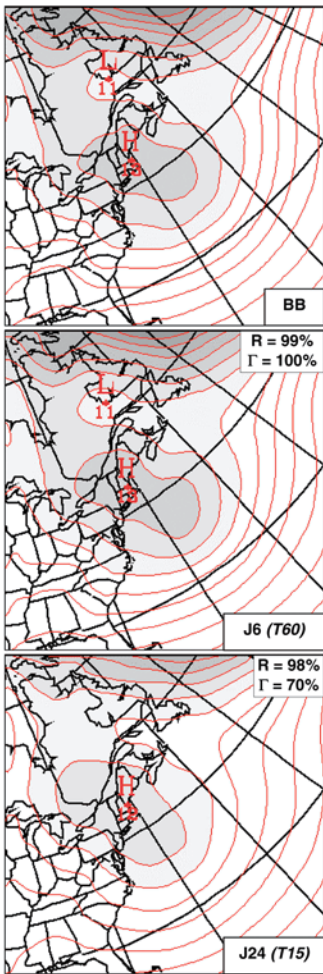


Fig. 10 Transient-eddy standard deviations of *slp*. Contours are at every 1.0 hPa. Areas with values larger than 10 hPa are shaded

Time averages of precipitation rates over the four February months are presented in Fig. 12. It can be seen that the Little Brother holds well up to J12. After that, the amount of precipitation decreases substantially, as can be seen on the J24 panel where the area receiving at least 2 mm per day has shrunk significantly. It can be noted that for all little-brother cases, precipitation is lower along the boundaries; the main reason for this is that the vertical velocity is set to zero at the boundaries. The stationary small-scale components are presented in Fig. 13. It can be seen that the time-averaging process has left negligible fine-scale features common to all simulations, especially over the ocean. But there are some signs of regional persistent precipitation patterns over the Great Lakes and over the sea-ice edge of the Labrador coast that are visible up to J24. In fact, when computed from land gridpoints alone for J24, the correlation coefficients increase from $R = 25\%$ to $R = 57\%$, and the variance ratio increases from $\Gamma = 81\%$ to $\Gamma = 92\%$.

The ability of the Little Brother to reproduce time variability of precipitation is shown in Figs. 14 and 15

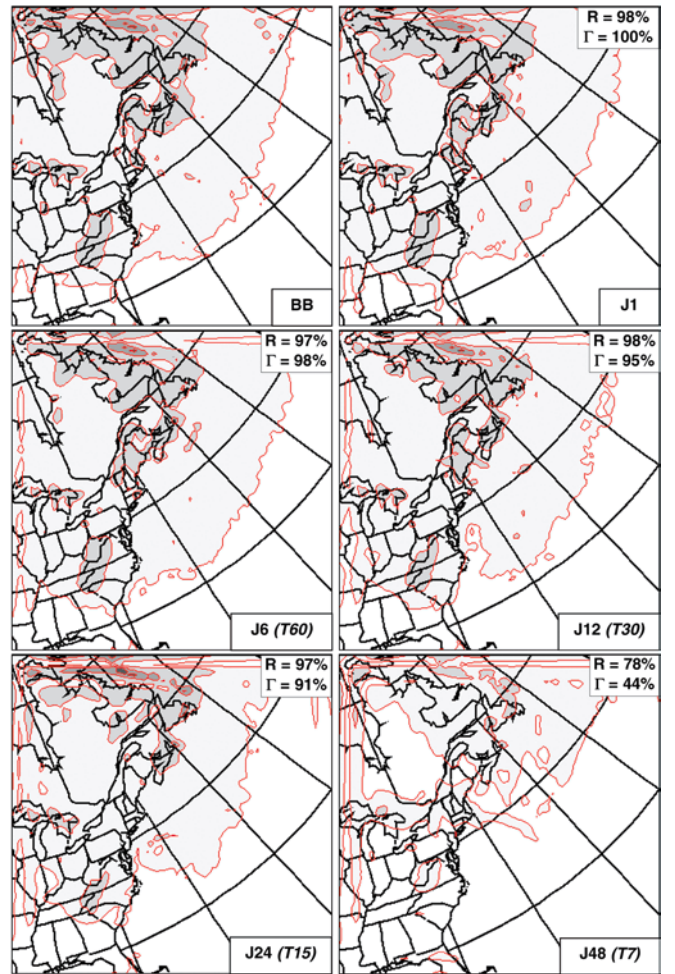


Fig. 11 Transient-eddy standard deviations of the small-scale component of *slp*. Contours are at every 0.2 hPa. Areas with values larger than 0.2 hPa are shaded

for the total and small-scale components, respectively. It can be noted, firstly, that both quantities have similar patterns and similar values (though somewhat smaller for the small-scale components). This is due to the fact that the temporal variance of the precipitation fields is dominated by the effect of transient fine-scale features such as fronts. Secondly, the maximum acceptable resolution jump ratio appears to be again J12.

3.1.3 Summary diagrams

A convenient graphical method to summarise comparisons of model results has been proposed by Taylor (2001). The Taylor diagram is a way of plotting on a 2-D graph, using the law of cosines (see Appendix), three statistics that indicate how closely two datasets match each other. These statistics make it easy to determine how much of the overall mean square difference (or root-mean-square difference) is attributable to a lack or excess of variance (or standard deviation) and how much is due to a poor pattern correlation. A diagram of

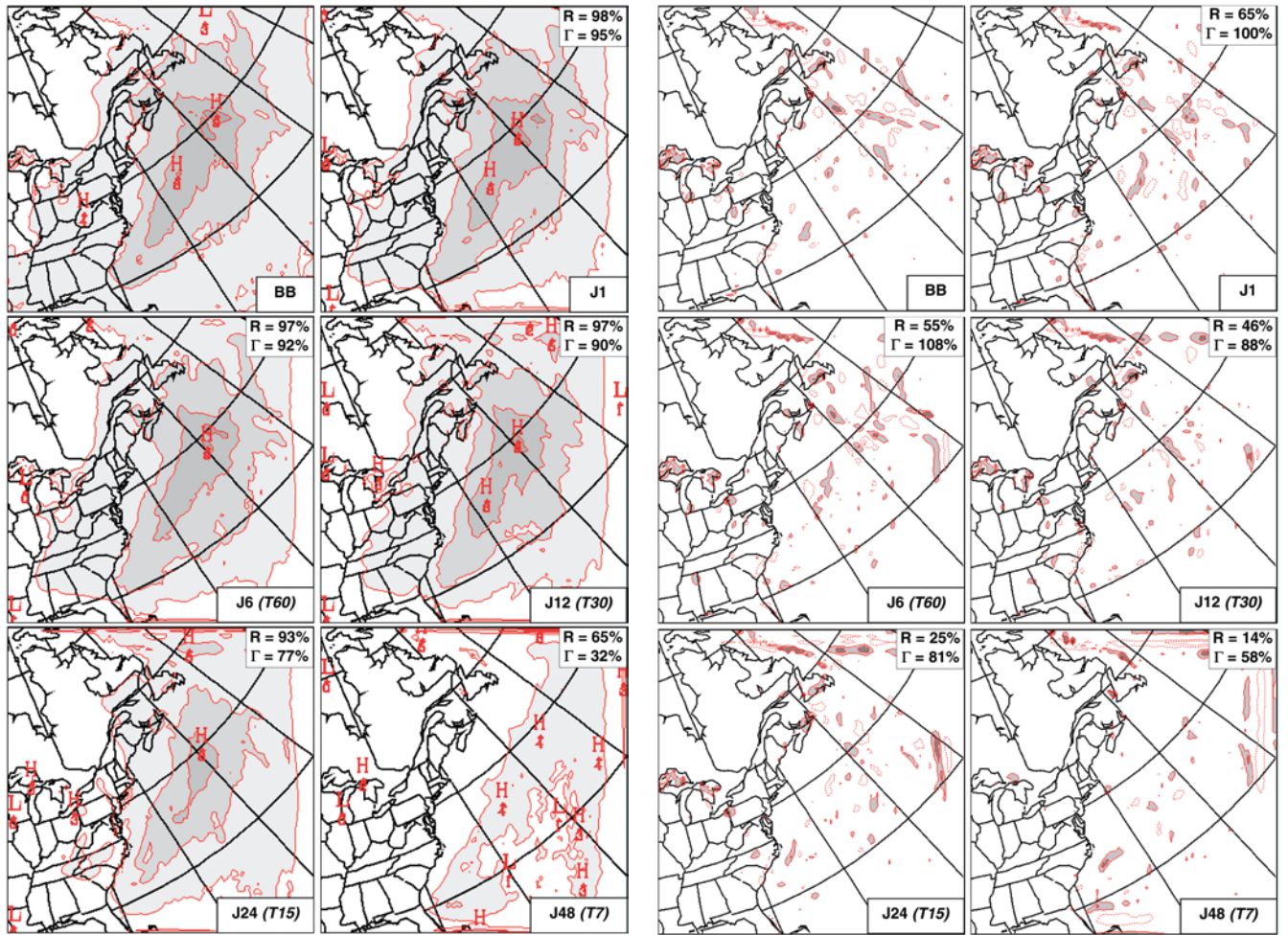


Fig. 12 Precipitation rates averaged over four February months. Contours are at every 2 mm per day. Areas with values larger than 2 mm per day are shaded

this type is shown in Figs. 16, 17. For a given point position on the diagram, the root-mean-square difference is proportional to the radial distance from the origin of the abscissa, the ratio of standard deviations (Little Brother/Big Brother) is proportional to the radial distance from the lower-right corner, and the correlation is the azimuthal position which gives the correlation coefficient between the Little and Big Brother. For normalisation purposes, the mean square difference is relative to the Big Brother's variance and thus expressed as a percentage. The goal for the Little Brother is to fall as close as possible to the abscissa origin with a ratio of variance near 100%. The space and time decomposition that was employed (see the Appendix) permits an evaluation of the little-brother performance in terms of the stationary (Fig. 16) and transient components (Fig. 17), respectively.

The expression for the stationary part is given by

$$\frac{d_{LB\overline{BB}}^{*2}}{\sigma_{\overline{BB}}^{*2}} = 1 + \frac{\sigma_{LB}^{*2}}{\sigma_{\overline{BB}}^{*2}} - 2 \frac{\sigma_{LB}^{*}}{\sigma_{\overline{BB}}^{*}} R_{LB\overline{BB}}^{*} \quad (1)$$

Fig. 13 Stationary small-scale component of precipitation rates. Contour intervals are $(-5, -3, -1, -0.5, 0.5, +1, +3, +5)$ mm day $^{-1}$. Regions with values larger than 0.5 mm day $^{-1}$ are shaded

where $d_{LB\overline{BB}}^{*2}/\sigma_{\overline{BB}}^{*2}$ is the relative mean square difference, $\sigma_{LB}^{*2}/\sigma_{\overline{BB}}^{*2}$ is the ratio of spatial variances, and $R_{LB\overline{BB}}^{*}$ is the correlation coefficient between the little-brother and the big-brother stationary part. The ratio of variance and the correlation coefficient for the stationary part in Eq. (1) are the same as those of Figs. 8–9 and Figs. 12–13.

The Taylor diagrams for the stationary component of the sea-level pressure, precipitation rate, 975-hPa temperature and 500-hPa relative vorticity are shown in Fig. 16. In each diagram, the results for the total fields and the fine-scale fields are displayed for the four resolution jump ratios as well as for the J1 case (NB: a ratio of one implies same resolution). It can be seen in all diagrams that the total fields are very robust to the increase of the resolution jump, at least up to J12 as shown by mean square differences smaller than 10% in all cases. This holds (although less strongly) also for the small-scale components of slp and temperature, but not for the precipitation and vorticity fields, which show a clear tendency to decorrelate and diminish variances with increasing resolution jumps.

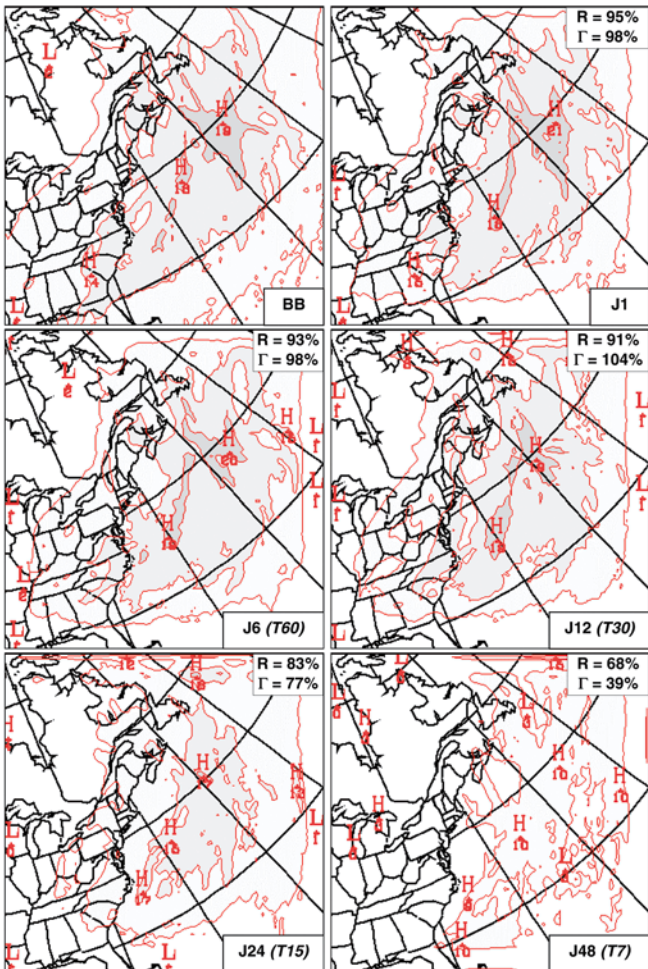


Fig. 14 Transient standard deviations of precipitation rates. Contours are at every 5 mm per day. Areas with values larger than 5 mm per day are shaded

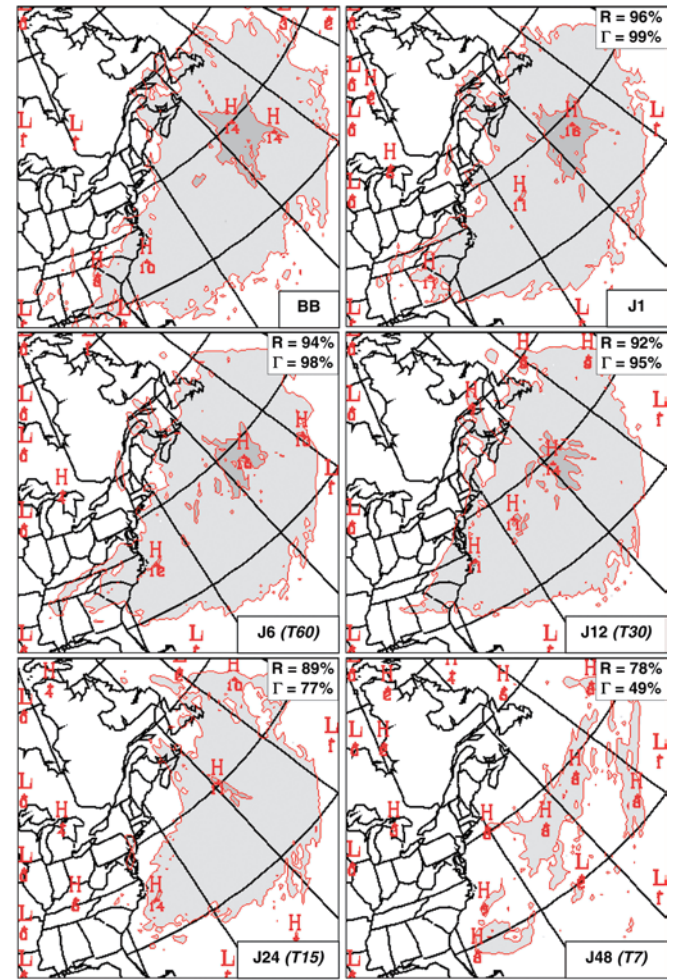


Fig. 15 Transient standard deviations of the small-scale component of the precipitation rates. Contours are at every 5 mm per day. Areas with values larger than 5 mm per day are shaded

The expression for the transient component is given by

$$\frac{\langle d_{LB\ BB}^2 \rangle}{\langle \sigma_{BB}^2 \rangle} = 1 + \frac{\langle \sigma_{LB}^2 \rangle}{\langle \sigma_{BB}^2 \rangle} - 2 \frac{\langle \sigma_{LB}^2 \rangle^{1/2}}{\langle \sigma_{BB}^2 \rangle^{1/2}} R'_{LB\ BB} \quad (2)$$

where $\frac{\langle d_{LB\ BB}^2 \rangle}{\langle \sigma_{BB}^2 \rangle}$ is the relative mean square difference of the transient part, $\frac{\langle \sigma_{LB}^2 \rangle}{\langle \sigma_{BB}^2 \rangle}$ is the ratio of the spatially averaged temporal variances, and $R'_{LB\ BB}$ is a temporal correlation coefficient. It must be noted that the ratio of variance and the correlation coefficient for the transient part as expressed in Eq. (2) are different than those shown in Figs. 10–11 and 14–15. In those figures, they represent scores computed from two 2-D images of the transient standard deviation while in Eq. (2), they are computed directly from two time series.

The Taylor diagrams for the transient components are displayed in Fig. 17. The *slp* and temperature fields are again the most reproducible fields by the Little Brother. The transient fine scales cause much more difficulty as it is apparent from the poor correlation in each diagram. This

is because our definition of the correlation coefficient for the transient component is deterministic, i.e. it takes into account the temporal correlation of events; that is very demanding for a climate model that is integrated for a longer period than the deterministic forecast period (a few days). Boer and Lambert (2001) have proposed a modified version of the Taylor diagram which is more adapted for global climate simulations. In effect, their mean square difference score is defined such that it is not influenced by the lack of temporal correlation expected after the deterministic period. In the case of a nested RCM, which is forced at the lateral boundaries, some temporal correlation is expected to occur at least for nested fields showing large-scale variances. On the other hand, the fine scales are not nested (for J6 to J48) and do not have to be time-correlated to yield a good climate. But their transient-eddy fields (e.g. Figs. 10–11 and Figs. 14–15) should correlate and have the same level of temporal variances. In other words, the poor correlation of the transient fine scales is not critical, but the decrease of variances as seen in Fig. 17 is. In this regard, the Little Brother does well up to J12 for all fields, except for the vorticity field.

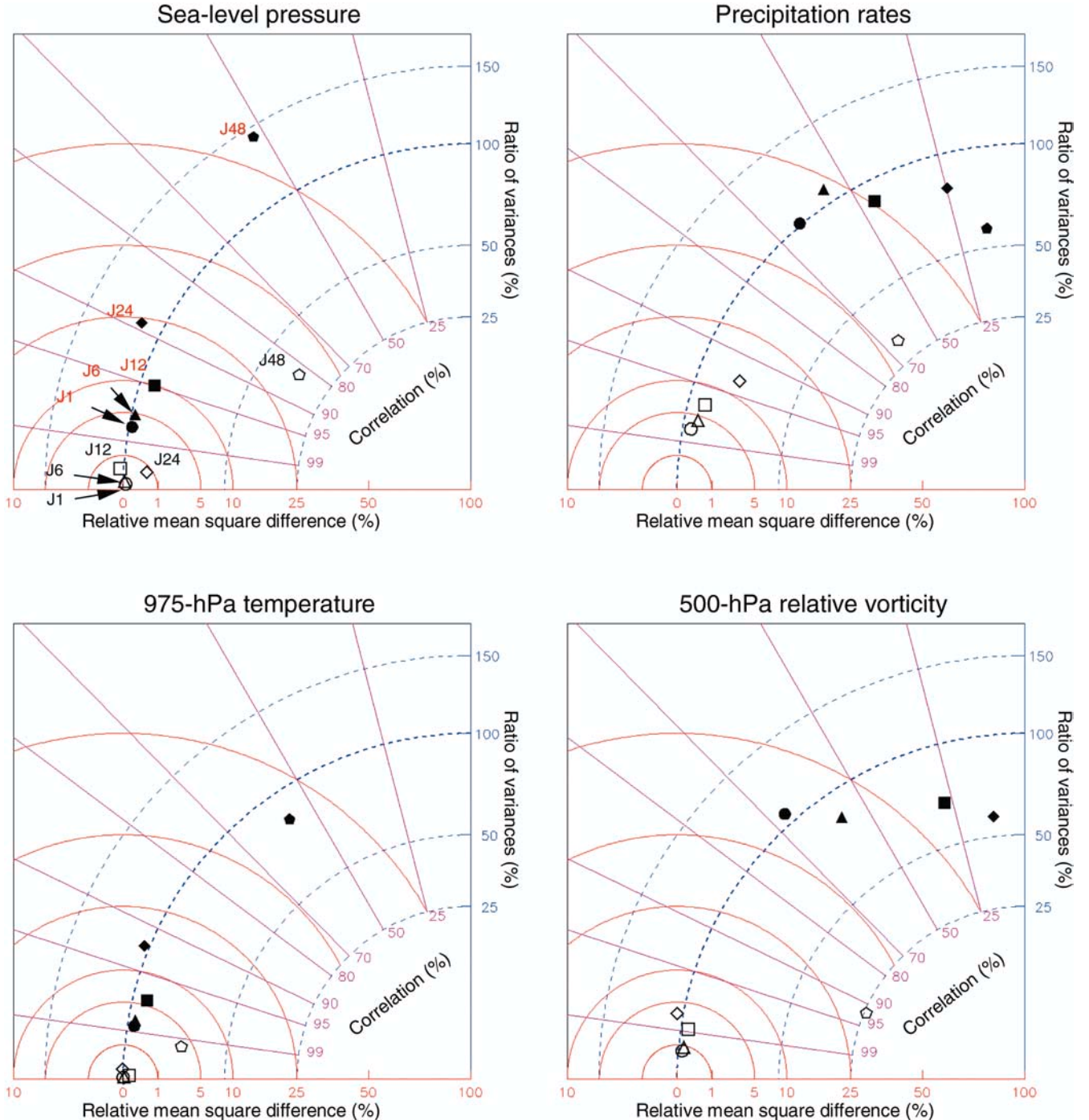


Fig. 16 Taylor diagrams showing the effect of the resolution jumps of the stationary component of the sea-level pressure, precipitation rates, 975-hPa temperature and 500-hPa vorticity fields. Circles: J1,

triangles: J6, squares: J12, diamonds: J24 and pentagons: J48. The open symbols are for the total fields and the filled ones are for their small-scale components only

3.2 Sensitivity to the temporal updating frequency

For this part of the study, the time interval of the nesting LBC data is varied, while no spatial filtering of the LBC is applied (J1 case). Four updating frequencies will be compared: U8, U4, U2 and U1, corresponding to 8, 4, 2 and 1 update per day, i.e. every 3, 6, 12 and 24 h, respectively. It should be noted that experiment U8

corresponds exactly to the experiment J1 presented earlier in Sect. 3.1.

As in the previous section, Taylor diagrams are used to synthesise the results. Figures 18, 19 summarise the effect of varying the updating frequency for the stationary and transient components, respectively. As can be seen in Fig. 18, the stationary component of the total fields that are strongly dominated by their large-scale

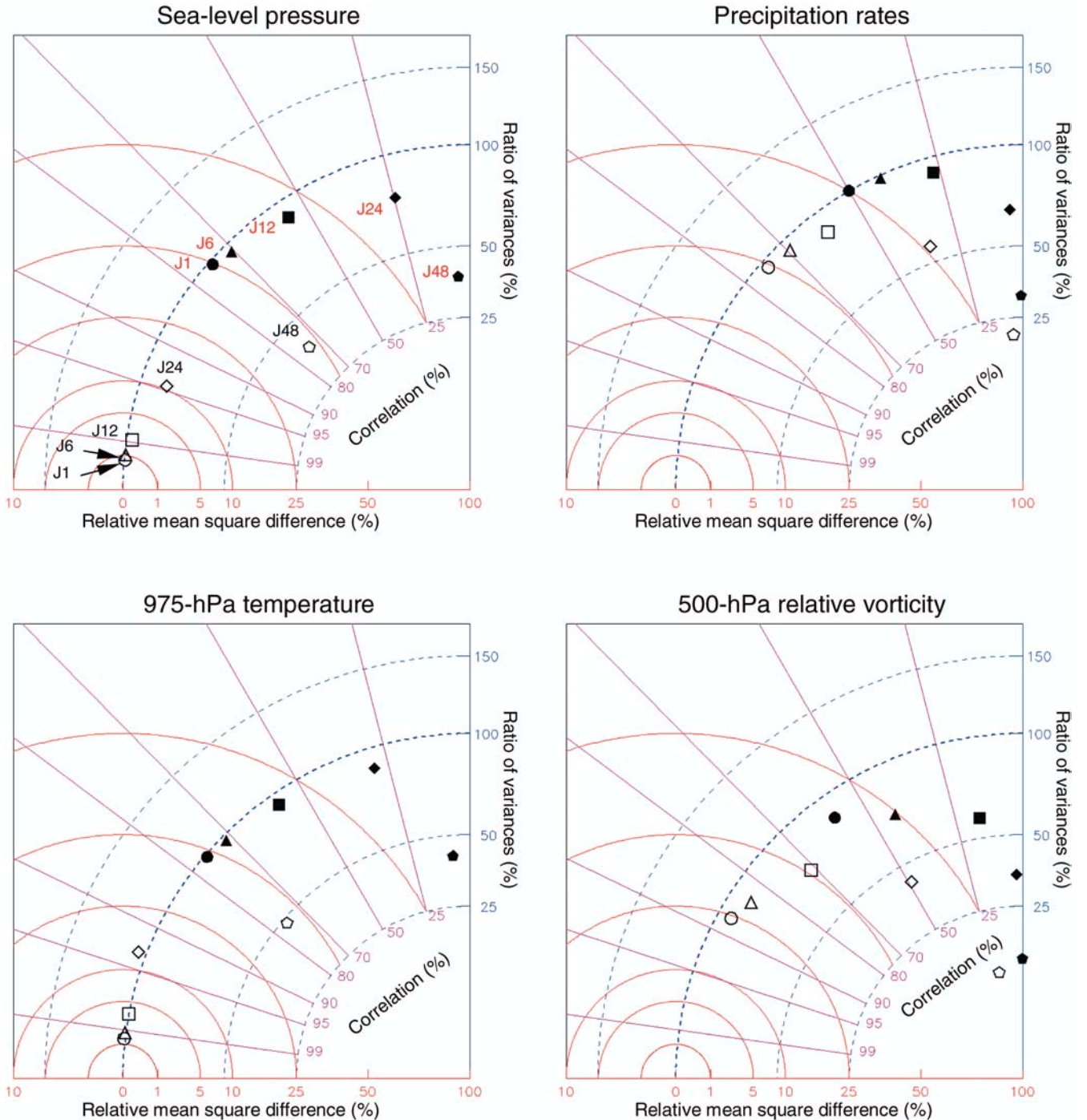


Fig. 17 Same as in Fig. 16, but for the transient component of the fields

variance (e.g. sea-level pressure and temperature) are not very sensitive. This may not be surprising since their large-scale components are slowly varying, therefore they do not require a very high temporal resolution of the LBC in order to be nested adequately. On the other hand, fields more dominated by fine-scale features, such as the precipitation and the vorticity fields, are more sensitive. This is especially true for fine-scale components as shown by the weak correlation, but it is not be

of much concern because the stationary components of these fields are weak (see for instance Fig. 13), and are not expected to correlate over regions lacking fine-scale surface forcings. Figure 18 also reveals that the mean square difference of the precipitation and vorticity have converged near 1% when the updating frequency is increased to eight times per day. Therefore, a totally errorless little-brother simulation does not seem reachable even with higher update frequencies. The reason for this

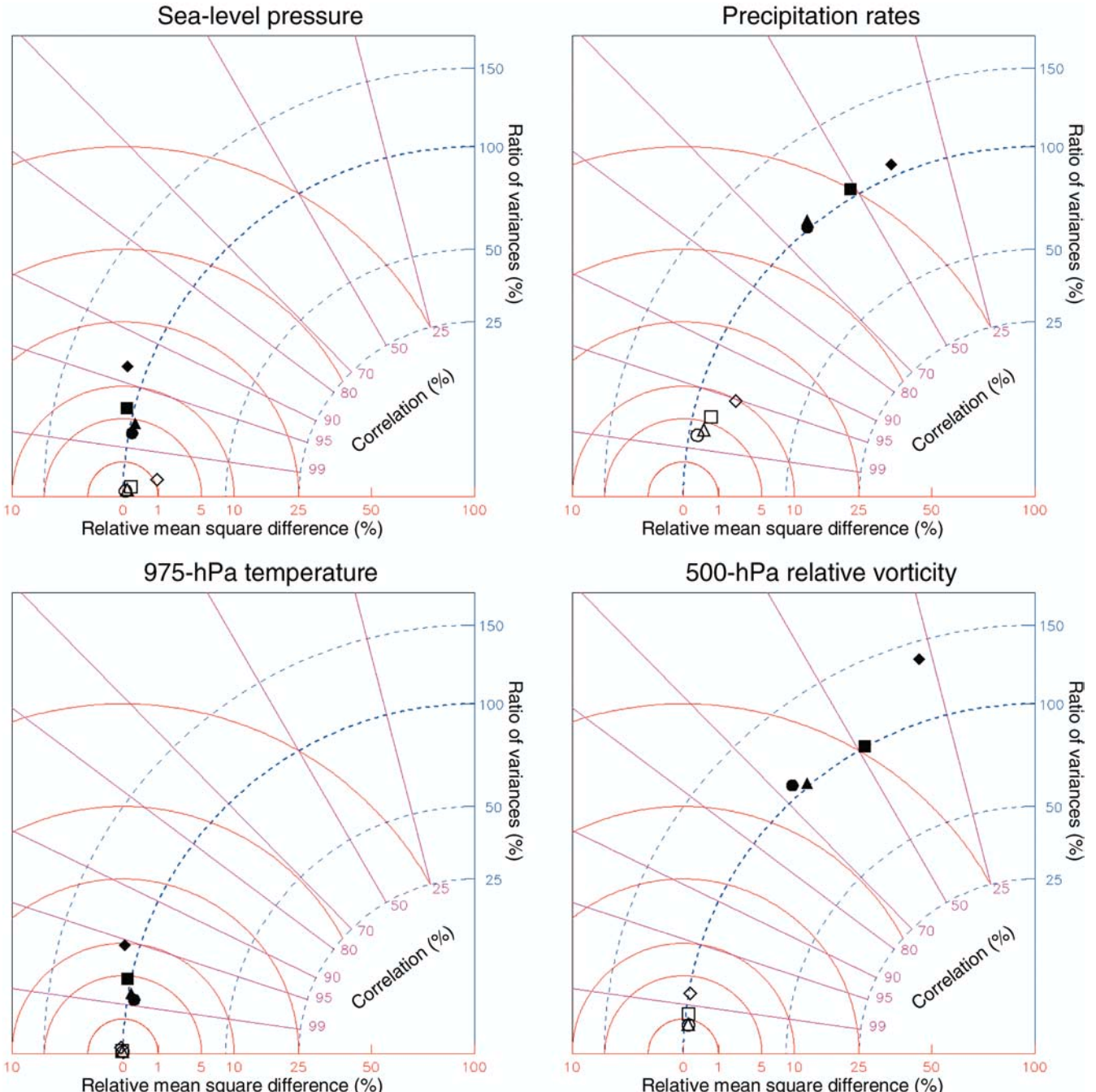


Fig. 18 Taylor diagrams showing the effect of update frequency on the stationary component of the sea-level pressure, precipitation rates, 975-hPa temperature and 500-hPa vorticity fields. Circles: U8

(3 h), triangles: U4 (6 h), squares: U2 (12 h), diamonds: U1 (24 h). The open symbols are for the total fields and the filled ones are for their small-scale components only

might be that other sources of errors, such as those generated by vertical interpolations performed for the nesting, are present in all cases and would not disappear even by updating every time step.

The impact of the update frequency on the transients is shown in Fig. 19. The precipitation and vorticity fields are more difficult to reproduce after U4 (6 h) and certainly after U2 (12 h), as apparent from the weaker temporal variance. This weakness is less pronounced for the sea-level pressure and is completely absent for

temperature. It is interesting to note that for all fields in Figs. 18, 19, the update intervals of 3 and 6 h yield similar results, as illustrated by the closeness of the circle and triangle symbols.

A last set of experiments has been performed in order to reflect more closely the spatial and temporal resolution of the LBC used in the current CRCM mode of operation which consists in driving an RCM at every 6 h with data provided by a spectral T32 GCM. For that purpose, a single resolution jump J12 (T30) has

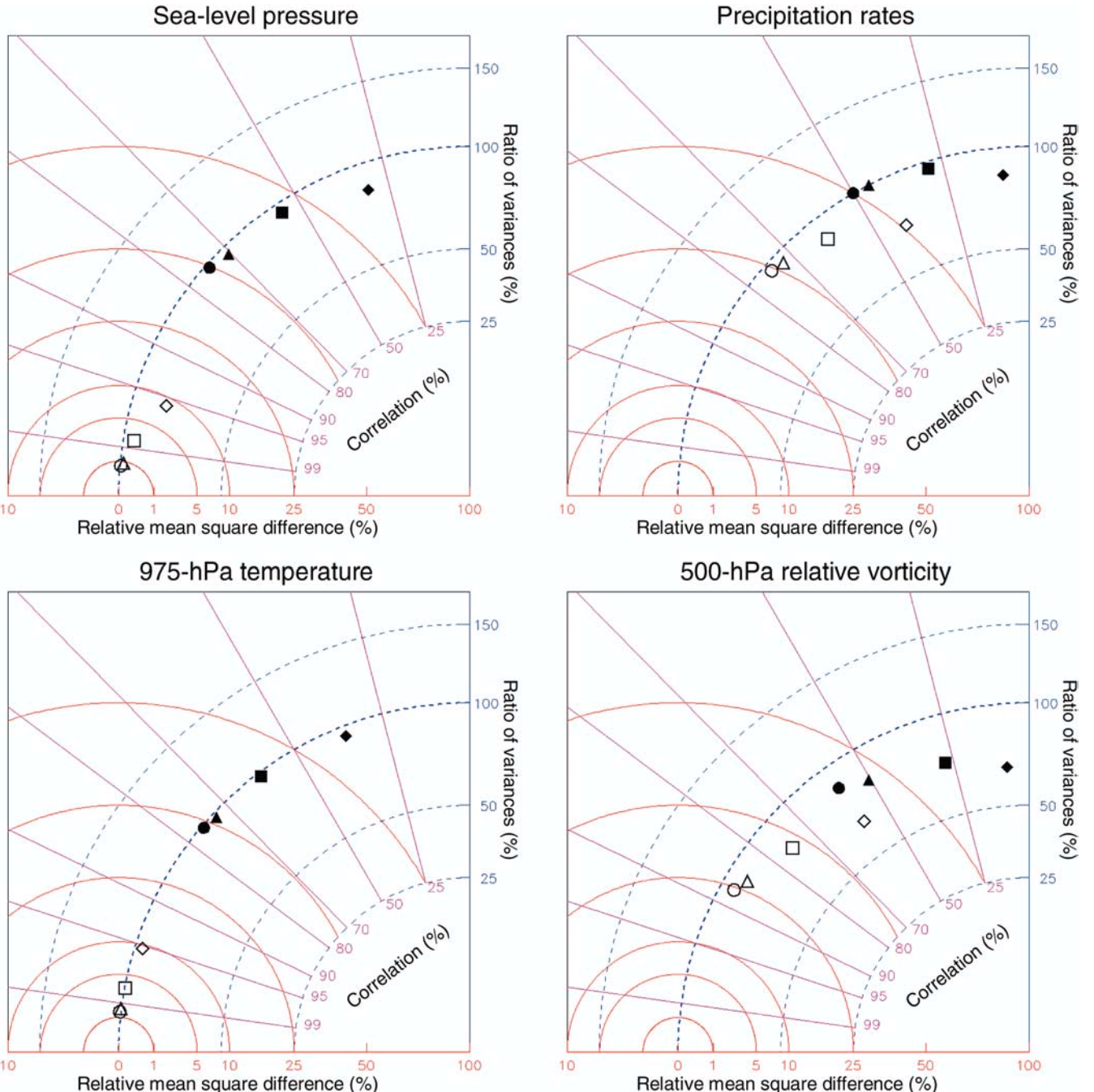


Fig. 19 Same as in Fig. 18, but for the transient component of the fields

been employed while the update frequency was varied. Figures 20, 21 show the results. It can be seen that the combination of resolution J12-U4, which is similar to what is currently used by the CRCM, gives satisfying results except for relative vorticity, for which the variance ratios of the transient components are significantly low. But it is clear, from the systematic closeness of the circles and triangles, that no gain can be obtained by diminishing the update interval from 6 to 3 hs. This simply reflects, in our BBE context, that driving data having a resolution equivalent to T30 contains only features that are large enough and travel slowly enough

to be resolved by a 6 h interval. On the other hand, reducing the resolution jump by using T60 driving data may likely requires shorter nesting intervals.

4 Discussion

The main hypothesis behind the use of a one-way nested RCM is that it can produce high-resolution climate information from low-resolution LBC, and can achieve this in a reliable and computationally efficient manner. The bigger the spatial resolution jump, the more efficient

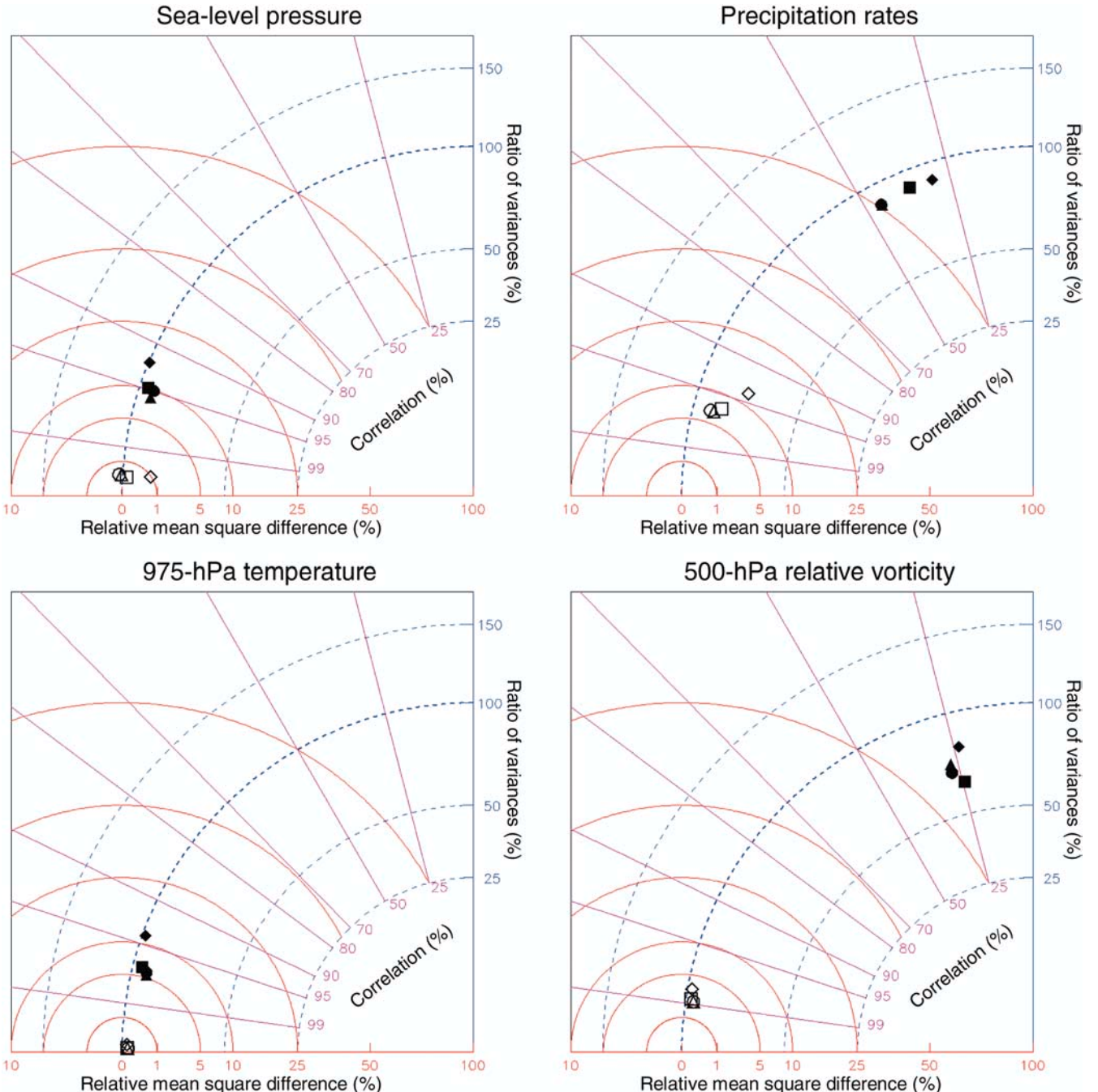


Fig. 20 Taylor diagrams showing the effect of update frequency for J12 on the stationary component of the sea-level pressure, precipitation rates, 975-hPa temperature and 500-hPa vorticity

this approach is; but this efficiency is at a cost of reliability. The same can be said for the updating frequency, but in this case a lower updating frequency means a reduced usage of storage space and data motion; this is usually a less stringent constraint than computation efficiency. In view of these considerations, let us review the results of the simulations performed in this research in order to define the upper limits of the spatial resolution jumps and update intervals for reliably running a one-way nested RCM.

fields. Circles: J12-U8, triangles: J12-U4, squares: J12-U2, diamonds: J12-U1. The open symbols are for the total fields and the filled ones are for their small-scale components only

The results concerning the impact of the spatial resolution jump at the lateral boundaries lead us to believe that jumps as high as 12 can be handled correctly by the nesting mechanism for a 45-km grid-point RCM, at least in a context of climate simulation where statistics such as the time mean and time variability are of primary importance. It must be noted that such a large resolution difference might be too much for deterministic weather forecasts, in particular when the fine-scale features are the centres of interest (Laprise et al. 2000; de Elía et al. 2002).

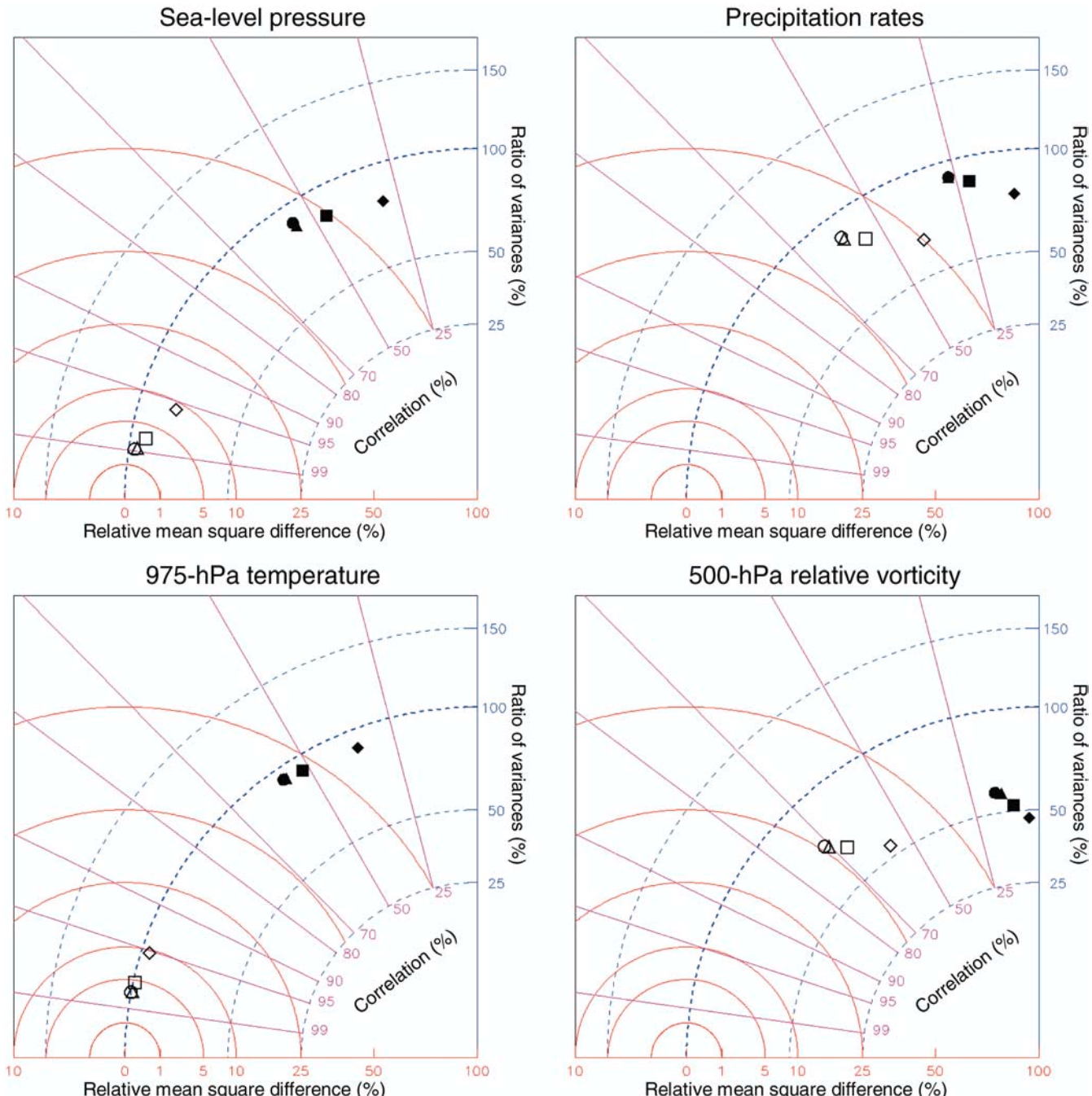


Fig. 21 Same as in Fig. 20, for the transient component of the fields

Concerning the maximum acceptable update time interval that can yield a reasonable climate, experiments showed that a 12-h interval is workable for a 45-km grid-point model but significant improvements are obtained by using a 6-h interval. Little improvement was gained by going from 6 to 3 h at this 45-km resolution. It is interesting to note that, during the infancy of the RCM science, time intervals of 12 h were the rule. This was probably because the computer storage necessary for archiving global climate simulations serving as driving data was too expensive, or because objective

analyses were only available at 12-h interval. Today, intervals of 6 h are currently used. It can be argued that update intervals longer than 6 or 12 h are too large to correctly capture synoptic systems that enter the domain and can underestimate fluxes across the lateral boundary (Majewski 1997). On the other hand, although such systems might not be quite resolved temporally at the lateral boundaries, they can be regenerated to a certain extent farther inside the domain (if it is large enough) by the large-scale dynamics which interact with the synoptic scales. A similar argument can be used to explain the

good results (up to J12) obtained in the first part when the LBC spatial resolution was degraded. However it seems that the larger the resolution differences or the update intervals are, the longer the fetch inside the nested domain should be to give enough room for the generation of transient fine-scale features. Unfortunately, this reduces the area of usefulness of the RCM domain, and so also its computational efficiency.

Using Taylor diagrams to visualise the results, it has been found that the transient components are more sensitive to the lack of resolution of the LBC (both temporal and spatial) than the stationary components since, as mentioned previously, fine-scale features not supplied at the inflow lateral boundaries must be regenerated inside the domain. Any deficiency with respect to this point should be reflected in the transient activity, especially for the smallest scales. On the other hand, stationary fine-scale features are largely caused by stationary forcings such as lakes and mountains, and for this reason show high robustness to the LBC resolution, as long as the large circulation that interacts with these forcings is well simulated overall. This can be seen, for instance, in Figs. 22, 23 which show the total and fine-scale components of the stationary 850-hPa wind fields, respectively. As long as the mean flow impedes the mountains with the correct speed and angle, or brings cold air masses over the warm open water areas, the Little Brothers are capable of reproducing the Big-Brother stationary fine scales.

The results indicate that the spatial and the temporal resolutions of the LBC impact jointly on the simulated climate. To further investigate this point, the most sensitive variable displayed on the Taylor diagrams, the variance ratio of the transient component of the total relative vorticity field, is used. Figure 24 displays the variance ratio as a function of resolution jump ratio and update interval. It can be seen that the isolines of variance ratio are concentric circles or ellipses, with quasi-horizontal lines at small update intervals and quasi-vertical lines at small resolution jumps. This means that the sensitivity to temporal resolution of the LBC is higher at small resolution jumps and decreases with larger resolution jumps because, in the latter case, high-frequency information is implicitly already absent from the low-resolution LBC. Similarly, the sensitivity to the resolution is high at high-frequency updates and decreases at lower frequencies. From Fig. 24, a characteristic “phase speed” can be computed by taking the ratio of the spatial wavelength to the temporal wavelength implied by the jumps and update intervals, respectively. The phase speed turns out to be 30–45 km/h, which is characteristic of the travelling weather systems in mid-latitudes during winter (Laprise and Zwack 1992). This means that the decrease of the transient variance found in the Taylor diagrams is probably due to the deficiency of adequately resolving weather systems that enter the domain and/or failing to fully regenerating them once inside.

Our finding, which shows that a spatial resolution jump of 12 (corresponding to T30 in our experiments)

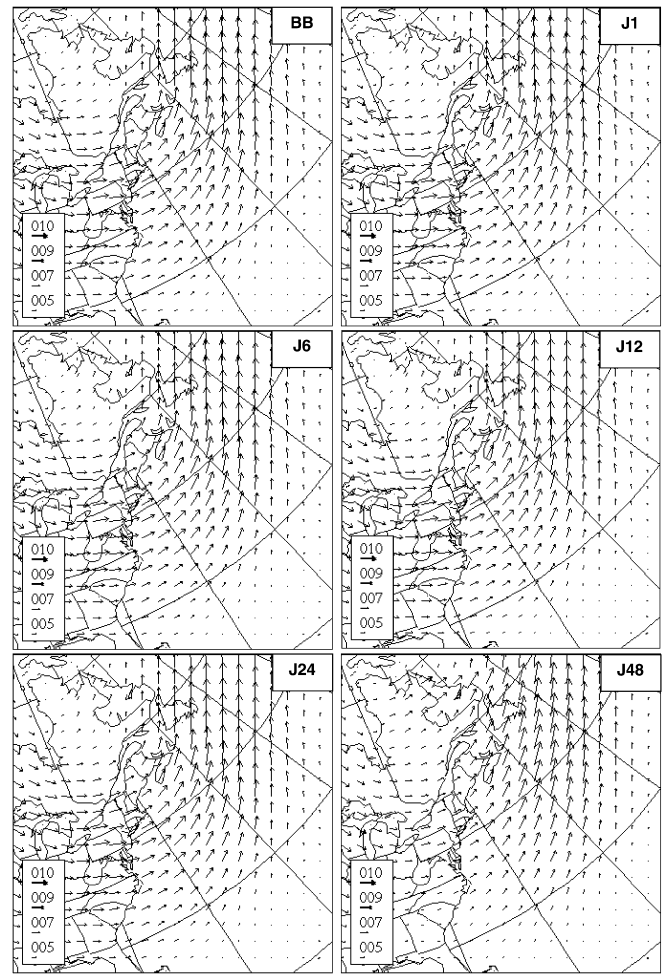
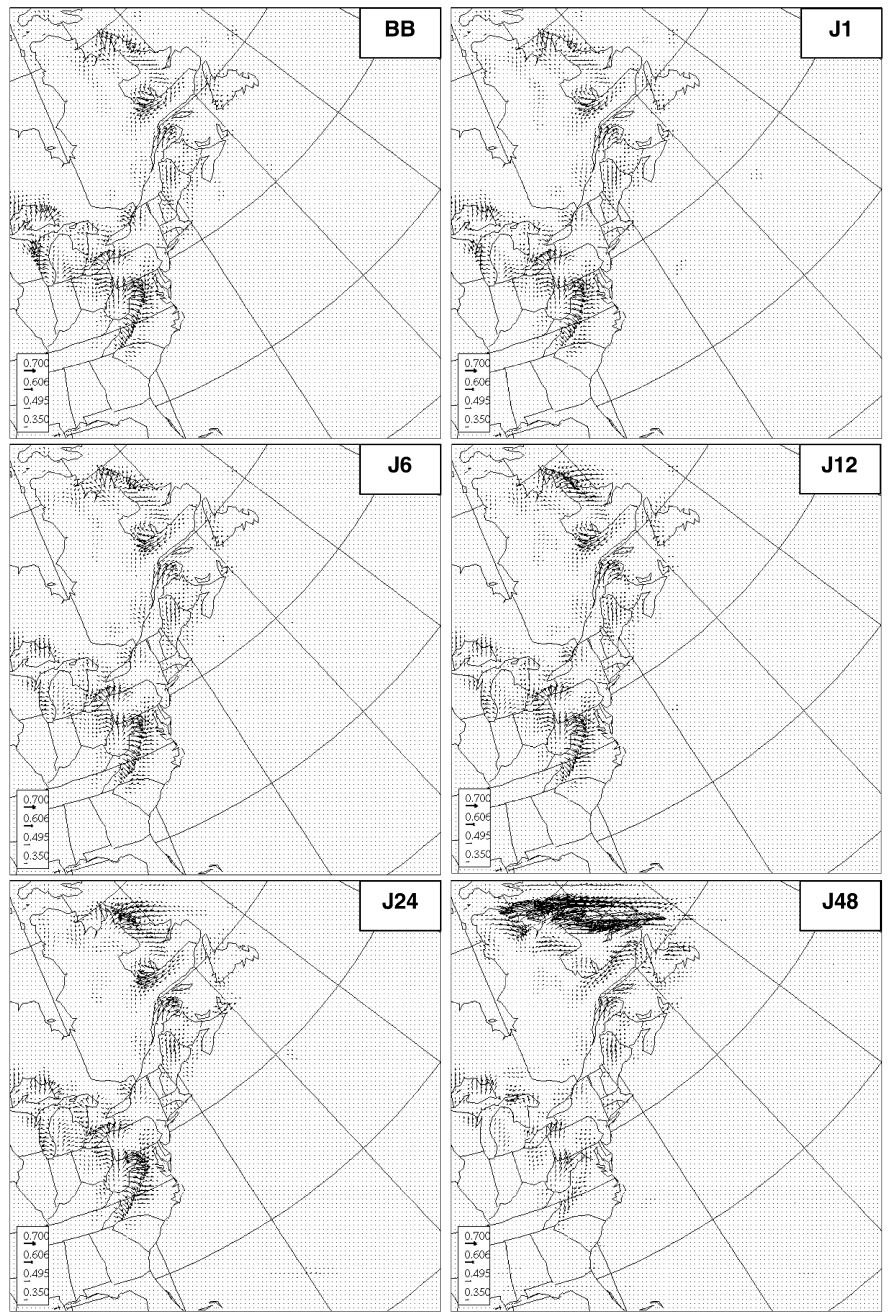


Fig. 22 Stationary component of the total 850-hPa wind fields (m s^{-1})

and an update frequency of four times per day (every 6 h) is acceptable for a 45-km grid-point RCM, must be seen as an upper limit since our BBE is a perfect prognosis approach, i.e. the reference truth is a model-generated virtual reality. The low-resolution data generated for the nesting of the Little Brother were, in a sense, perfect since the full model resolution participated in its generation. This would not be the case for a GCM run at very low resolution such as T7. In effect, a T7 GCM does not produce an acceptable climate even for the large-scale atmospheric circulation since important smaller scale interactions are absent; they are required for the GCM to yield a good large-scale climate. This has been demonstrated by Boer and Denis (1997) who showed that the large-scale solution of a GCM does not converge below T32 resolution. Therefore nesting an RCM with a low-resolution GCM might yield worse results than those seen in this study. Furthermore, in real applications, nested RCMs often do not share the same dynamical numerics and/or physical parametrisation with the driving model (or analyses). Even when this is, or nearly is the case, the fact that the driving model and the RCM are not run at the same physical spatial

Fig. 23 Stationary component of the fine-scale component of the 850-hPa wind fields (m s^{-1})



resolution (grid-point spacing or spectral truncation) may lead to different behaviour in the two model versions. In effect, the dynamical part of each model may lead to dissimilar phase speeds of travelling weather systems resulting in a mismatch at the lateral boundaries. This may call for higher updating frequency or for a domain-wide control of the largest scales that guide the evolution of the synoptic systems (see Biner et al. 2000; von Storch et al. 2000 on this topic). The physical parametrisations may also cause problems even if they are the same because they may have different responses to the spatial resolution. Our BBE does not address these issues because the grid-point spacings were the same between the Big and the Little Brothers. In fact, the BBE was

designed precisely to eliminate these effects in order to concentrate solely on the nesting, without having to sort out the effects just mentioned. Nevertheless, these issues and others, such as the effect of the domain size, the domain location, the season and whether or not an RCM should improve the large-scale circulation of its driving model, will ultimately have to be addressed. However, from the present results, we can tentatively speculate about the effect of the domain location and the seasons. In effect, we saw that the surface forcings, such as mountains and lakes, were in large part responsible for the downscaling ability of the RCM, at least for the stationary phenomena. Thus, a domain located over such regions (the Rockies for instance), should yield to

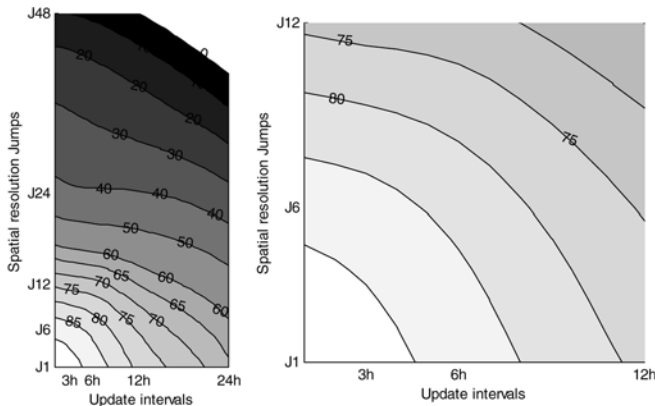


Fig. 24 **a** Ratios of the variance of transient-eddy relative vorticity between the Little and Big Brother as a function of the spatial resolution jumps and update intervals of the lateral boundary conditions. **b** Is an enlargement of the lower-left corner of plot **a**. The isolines have been generated by fitting the simulated-results statistics

better results than over homogeneous terrain. Secondly, since classical one-way nested RCMs are driven by the forcing exerted only at the lateral boundaries, weaker large-scale circulation that prevails during the summer season might not provide enough constraint on the RCM interior solution to keep it from diverging from the driving large-scale solution.

Finally, a successful BBE test must be viewed as a necessary but not sufficient condition to prove without any doubts that the one-way nesting RCM approach is a reliable approach.

5 Conclusion

Our goal was to shed some light on two of the most important issues concerning the use of one-way nested RCMs as a downscaling climate technique: the impacts of the *spatial* resolution and *temporal* updating frequency of the lateral boundary conditions. To address these issues, a perfect-prognosis framework called the Big-Brother Experiment, developed by Denis et al. (2002b), was employed. This framework consists in using the same model to produce both the control and nested simulations. This approach allowed us to address the issues separately without mixing nesting errors with those due to possible different formulations between the driving and the nested model. Using this framework with a 45-km grid-point RCM over the North American east coast and during winter months, it has been found that:

1. Spatial resolution jump ratios up to 12 between the resolution of the nesting LBC data and the RCM can yield reliable regional climate for most fields studied with an RCM at 45 km resolution.
2. Update frequency of twice a day (every 12 h) are almost sufficient although 6 h is significantly better and should be used since there is little increase of

computational cost related to doing so. No improvement was found by going from 6 to 3 h in our tests with a 45-km grid-point RCM.

3. Although the 500-hPa relative vorticity was the most affected variable when the resolution of the LBC was degraded, the most important climate fields, such as those of the precipitation, temperature, and sea-level pressure fields were far less affected. These last two fields showed the most resistance to the LBC resolution degradation; their largest scales did not need a high-resolution LBC to be well nested, and their stationary fine-scale components are, in turn, strongly forced by the surface heterogeneities and therefore rather independent of the LBC.
4. The combination of T32-6 hours currently employed in the Canadian RCM mode of operation seems acceptable, although significant improvements can be anticipated by reducing the spatial resolution jump ratio to 6 from 12, i.e. by the use of T60 resolution driving data.

Lastly, additional work needs to be done to investigate how these conclusions may apply to other domain sizes, locations, seasons. It would also be interesting to see how the present results can be carried over to other models and at resolutions other than 45-km grid spacing.

Acknowledgements This work has been financially supported by funding from the Climate Change Prediction Program (CCPP) of the US Department of Energy, and from the UQAM regional climate modelling group. We gratefully acknowledge the Meteorological Service of Canada for granting an education leave to the first author during this study and for providing access to its facilities. We thank the UQAM regional climate modelling staff for their invaluable technical help with the Canadian RCM. We also thank Dr. Bernard Dugas, Dr. Ramón de Elía and M. Richard Harvey for stimulating discussions.

Appendix 1

Development of the space-time decomposition for the Taylor diagrams

We describe the space-time decomposition performed to compare the stationary and transient components of two model runs in Taylor diagrams. Following a commonly used procedure in climate studies, a spatially and time-varying field $\psi(x, y, t)$ is decomposed in space as:

$$\psi(x, y, t) = \langle \psi \rangle(t) + \psi^*(y, y, t) , \quad (3)$$

and time as:

$$\psi(x, y, t) = \bar{\psi}(x, y) + \psi'(y, y, t) , \quad (4)$$

where the brackets and the overbar denote a space (horizontal domain here) and time-average operator, respectively. Combining Eqs. (3) and (4) yields to a standard space-time decomposition

$$\psi(x, y, t) = \langle \bar{\psi} \rangle + \bar{\psi}^*(x, y) + \psi'(x, y, t) , \quad (5)$$

where $\langle \bar{\psi} \rangle$ is the overall mean; $\bar{\psi}^*$ and ψ' are termed the stationary eddy and transient eddy components, respectively.

Using this decomposition, the space-time mean square difference of two time series of two-dimensional spatial fields $A = A(x, y, t)$ and $B = B(x, y, t)$ can be expressed as

$$\langle \overline{d_{AB}^2} \rangle \equiv d_{\langle A \rangle \langle B \rangle}^2 + d_{AB}^{*2} + \langle \overline{d_{AB}^r} \rangle = \langle \overline{(A - B)^2} \rangle , \quad (6)$$

where

$$d_{\langle A \rangle \langle B \rangle}^2 \equiv (\langle \bar{A} \rangle - \langle \bar{B} \rangle)^2 \quad (7)$$

is the difference in the overall means,

$$d_{AB}^{*2} = \langle \overline{\bar{A}^{*2}} \rangle + \langle \overline{\bar{B}^{*2}} \rangle - 2\langle \bar{A}^* \bar{B}^* \rangle \quad (8)$$

is the difference in the stationary eddy component, and

$$\langle \overline{d_{AB}^r} \rangle = \langle \overline{A'^2} \rangle + \langle \overline{B'^2} \rangle - 2\langle \overline{A' B'} \rangle \quad (9)$$

is the difference in the transient eddy components.

Equation (8) can be reformulated in terms of spatial variances and correlation since

$$\sigma_A^{*2} \equiv \langle (\bar{A} - \langle \bar{A} \rangle)^2 \rangle = \langle \overline{\bar{A}^{*2}} \rangle ; \quad (10)$$

$$\sigma_B^{*2} \equiv \langle (\bar{B} - \langle \bar{B} \rangle)^2 \rangle = \langle \overline{\bar{B}^{*2}} \rangle ; \quad (11)$$

$$R_{AB}^* \equiv \frac{\langle (\bar{A} - \langle \bar{A} \rangle)(\bar{B} - \langle \bar{B} \rangle) \rangle}{\sigma_A^{*2} \sigma_B^{*2}} = \frac{\langle \overline{\bar{A}^* \bar{B}^*} \rangle}{\sigma_A^{*2} \sigma_B^{*2}} , \quad (12)$$

giving

$$d_{AB}^{*2} = \sigma_A^{*2} + \sigma_B^{*2} - 2\sigma_A^* \sigma_B^* R_{AB}^* \quad (13)$$

For the transient eddy components of the mean square difference (Eq. 9), we define these variances and correlation coefficient:

$$\langle \sigma_A^2 \rangle \equiv \langle \overline{(A - \bar{A})^2} \rangle = \langle \overline{A'^2} \rangle , \quad (14)$$

$$\langle \sigma_B^2 \rangle \equiv \langle \overline{(B - \bar{B})^2} \rangle = \langle \overline{B'^2} \rangle , \quad (15)$$

$$R'_{AB} \equiv \frac{\langle \overline{A' B'} \rangle}{\langle \overline{A'^2} \rangle^{1/2} \langle \overline{B'^2} \rangle^{1/2}} = \frac{\langle \overline{A' B'} \rangle}{\langle \sigma_A^2 \rangle^{1/2} \langle \sigma_B^2 \rangle^{1/2}} , \quad (16)$$

giving

$$\langle \overline{d_{AB}^r} \rangle = \langle \sigma_A^2 \rangle + \langle \sigma_B^2 \rangle - 2\langle \sigma_A^2 \rangle^{1/2} \langle \sigma_B^2 \rangle^{1/2} R'_{AB} \quad (17)$$

Equations (13) and (17) can be conveniently represented in the Taylor diagram, which exploits their similarity with the law of cosine

$$c^2 = a^2 + b^2 - 2ab \cos(\phi) . \quad (18)$$

For convenience, the stationary and transient expressions are normalised by their respective variances of $B(x, y, t)$ such that identical simulations will show up on the diagram as a point located on the abscissa at unit distance from the origin (i.e. same variances and a correlation coefficient of 100%). These final expressions for the stationary and transient components are given by

$$\frac{d_{AB}^{*2}}{\sigma_B^{*2}} = 1 + \frac{\sigma_A^{*2}}{\sigma_B^{*2}} - 2\frac{\sigma_A^*}{\sigma_B^*} R_{AB}^* \quad (19)$$

and

$$\frac{\langle \overline{d_{AB}^2} \rangle}{\langle \sigma_B^2 \rangle} = 1 + \frac{\langle \sigma_A^2 \rangle}{\langle \sigma_B^2 \rangle} - 2\frac{\langle \sigma_A^2 \rangle^{1/2}}{\langle \sigma_B^2 \rangle^{1/2}} R'_{AB} \quad (20)$$

respectively.

References

- Bergeron G, Laprise R, Caya D (1994) Formulation of the Mesoscale Compressible Community (MC2) model. Cooperative Centre for Research in Mesometeorology, 165 pp (Available from Dr. D. Caya, Groupe des Sciences de l'Atmosphère, Département des Sciences de la Terre et de l'Atmosphère, Université du Québec à Montréal, C.P. 8888, Succursale "Centre-Ville," Montréal, PQ, H3C 3P8, Canada)
- Biner S, Caya D, Laprise R, Spacek L (2000) Nesting of RCMs by imposing large scales. In: Research activities in atmospheric and oceanic modelling, WMO/TD-987, Rep 30: 7.3–7.4
- Boer GJ, Denis B (1997) Numerical convergence of the dynamics of a GCM. *Clim Dyn* 13: 359–374
- Boer GJ, Lambert SJ (2001) Second-order space-time climate difference statistics. *Clim Dyn* 17: 213–218
- CAS/JSC WGNE (1999) Report of Fourteenth Session of the CAS/JSC Working Group on Numerical Experimentation (Recherche en Prévision Numérique, Environnement Canada, Doval, Québec, Canada, 2–6 November 1998). Number 14, WMO/TD-964, World Meteorological Organization, pp 28
- CAS/JSC WGNE (2000) Report of Fifteenth Session of the CAS/JSC Working Group on Numerical Experimentation (Naval Research Laboratory, Monterey, CA, USA, 25–29 October 1999). Number 15, WMO/TD-24, World Meteorological Organization, pp 29
- Caya D, Laprise R (1999) A semi-implicit semi-Lagrangian regional climate model: the Canadian RCM. *Mon Weather Rev* 127: 341–362
- Davies HC (1976) A lateral boundary formulation for multi-level prediction models. *Q J R Meteorol Soc* 102: 405–418
- de Elía R, Laprise R, Denis B (2002) Forecasting skill limits of nested, limited-area models: a perfect-model approach. *Mon Weather Rev* 130: 2006–2023
- Denis B, Côté J, Laprise R (2002a) Spectral decomposition of two-dimensional atmospheric fields on limited-area domains using discrete cosine transforms (DFT). *Mon Weather Rev* 130: 1812–1829
- Denis B, Laprise R, Caya D, Côté J (2002b) Downscaling ability of one-way nested regional climate models: The big-brother experiment. *Clim Dyn* 18: 627–646
- Giorgi F, Mearns LO (1999) Introduction to special section: regional climate modeling revisited. *J Geophys Res* 104: 6335–6352
- Kain JS, Fritsch JM (1990) A one-dimensional entraining/detraining plume model and its application in convective parameterization. *J Atmos Sci* 47: 2784–2802
- Laprise R, Zwack P (1992) Variation de l'activité cyclonique dans un scénario double CO₂. *Le Climat* 10: 39–62
- Laprise R, Caya D, Bergeron G, Giguère M (1997) The formulation of André Robert MC2 (Mesoscale Compressible Community) model. The André J. Robert Memorial Volume (Lin C, Laprise R, Ritchie H, eds), companion volume to *Atmos–Ocean* 35: 195–220
- Laprise R, Caya D, Giguère M, Bergeron G, Côté H, Blanchet J-P, Boer G, McFarlane AN (1998) Climate and climate change in western Canada as simulated by the Canadian regional climate model. *Atmos–Ocean* 36: 119–167
- Laprise R, Ravi Varma MK, Denis B, Caya D, Zawadzki I (2000) Predictability in a nested limited-area model. *Mon Weather Rev* 128: 4149–4154
- Majewski D (1997) Operational regional prediction. *Meteorol Atmos Phys* 63: 89–104

- McFarlane NA, Boer GJ, Blanchet J-P, Lazare M (1992) The Canadian Climate Centre second-generation general circulation model and its equilibrium climate. *J Clim* 5: 1013–1044
- Paquin D, Caya D (2001) New convection scheme in the Canadian Regional Climate Model. In: Research activities in Atmospheric and Oceanic Modelling, WMO/TD-987, Rep 30: 7.14–7.15
- Robert A, Yakimiw E (1986) Identification and elimination of an inflow boundary computational solution in limited area model integrations. *Atmos–Ocean* 24: 369–385
- Taylor KE (2001) Summarizing multiple aspects of model performance in a single diagram. *J Geophys Res* 106: 7183–7192
- von Storch H, Langenberg H, Feser F (2000) A spectral nudging technique for dynamical downscaling purposes. *Mon Weather Rev* 128: 3664–3673
- Yakimiw E, Robert A (1990) Validation experiments for a nested grid-point regional forecast model. *Atmos–Ocean* 28: 466–472